Article

An Analytical Model with Three Sub-Regions for M₂ Tide in the Yellow Sea and the East China Sea

Kyung Tae Jung[1]*, Chang Wook Park[2], Im Sang Oh[2], and Jae Kwi So[1]

[1]*Ocean Energy & Environmental Engineering Research Division, KORDI, Ansan P.O. Box 29, Seoul 425-600, Korea*
[2]*School of Earth and Environmental Science, College of Natural Sciences, Seoul National University, Seoul 151-747, Korea*

Abstract – In this study an analytical tide model of uniform width with three sub-regions is presented. The three-subregions model takes into account step-like variations in depths in the direction of the channel as a way to examine the M_2 tide of the East China Sea (ECS) as well as the Yellow Sea (YS). A modified Proudman radiation condition has been applied at the northern open head, while the sea surface elevation is specified at the southern open boundary. It is seen that, due to the presence of an abrupt change in depth, co-amplitude lines of the M_2 tide are splitted to the east and west near the end of the ECS shelf region. Variations in depths, bottom friction and the open head boundary conditions all contribute to the determination of formation of amphidromes as well as overall patterns of M_2 tidal distribution. It is seen that increasing water depth and bottom friction in the ECS shelf results in the westward shift of the southern amphidrome. There is however no hint at all of the well-known degenerated tidal pattern being formed. It is inferred that a lateral variation of water depth has to be somehow incorporated to represent the tidal patterns in ECS in a realistic manner. Regarding the radiation factor introduced by Fang *et al.* (1991), use of a value larger than one, possibly with a phase shift, appears to be a proper way of incorporating the reflected waves from the northern Yellow Sea (NYS).

Key words – analytical model, M_2 tide, Kelvin wave, Yellow Sea, East China Sea

1. Introduction

As a way of gaining insight on the co-oscillating tide in the Yellow Sea, analytical models have been developed in the past based on Taylor's solution (Kang 1984; Fang *et al.* 1994; Kang *et al.* 1999; So 2000). In a pioneering work by

*Corresponding author. E-mail: ktjung@kordi.re.kr

Kang (1984) the Yellow Sea was represented as a frictionless, semi-infinite channel with partial opening at the head. At the open head, a free radiation condition called POBC (Proudman open boundary condition) was applied. Fang *et al.* (1991) presented a frictional, finite channel model for the Yellow Sea with partial reflection at the northern open head and with specification of sea surface elevation at the southern boundary. Kang *et al.* (1999) extended the model developed by Kang (1984) by including the bottom friction. So (2000) presented solutions with a set of forced radiation conditions (for example, Reid and Bodine (1968), Flather (1976) and Blumberg and Kantha (1985) radiation conditions) at the northern open head. In the North Sea Brown (1987) derived a solution with use of an oscillating current boundary condition in the English Channel. In all these studies, the channel width and depth are however assumed to be constant. That is, previous analytical models are mainly concerned with the investigation of tidal structure in the YS region.

In this paper, a finite channel model with three sub-regions of equal width is presented in which each sub-region might have a different value of water depth and/or a bottom frictional coefficient, covering the model region up to the Ryukyu Islands where the water depth reaches more than 1000 m. Although the model presented in this study is far different from the realistic situation in that the open water east of the ECS is assumed to be blocked by a straight coastline and the water depth variation is neglected, it might be interesting to investigate the influence of the abrupt depth change near the bottom of the ECS on the tidal pattern and the possible cause of the formation of

the degenerated amphidromic pattern on the Chinese side in ECS. The continuity of sea surface elevation and flux are imposed at the interfaces between sub-regions along with the conventional treatment of the northern head and southern open boundaries of the channel. These matching approaches were used by Godin (1965) in constructing a three sub-region analytical model for the M_2 tide in the Labrador Sea and by Webb (1976) in constructing a two sub-region model for tidal oscillation off the east coast of Australia. We also present some recent efforts of further extending the present model by taking into account the variations in channel width in a step-like manner.

2. The Model

Governing equations and general solutions

The linear shallow water equations governing tidal motion in Cartesian coordinates are

$$\frac{\partial \tilde{u}}{\partial t} - f\tilde{v} = -g\frac{\partial \tilde{\zeta}}{\partial x} - \gamma\tilde{u} \tag{1}$$

$$\frac{\partial \tilde{v}}{\partial t} + f\tilde{u} = -g\frac{\partial \tilde{\zeta}}{\partial y} - \gamma\tilde{v} \tag{2}$$

$$\frac{\partial \tilde{\zeta}}{\partial t} = -h\left(\frac{\partial \tilde{u}}{\partial x} + \frac{\partial \tilde{v}}{\partial y}\right) \tag{3}$$

where t represents time, $\tilde{u}$, $\tilde{v}$ are the velocity components to x and y directions, respectively, $\tilde{\zeta}$ is the elevation of the free surface, g is the acceleration of gravity, h is the depth, γ is the bottom frictional coefficient and f is the Coriolis parameter.

Assuming that the motion is periodic in time, we may then write

$$(\tilde{\zeta}, \tilde{u}, \tilde{v}) = Re(\zeta, u, v)e^{i\sigma t} \tag{4}$$

where σ is the angular frequency of oscillation, ζ, u and v are the complex-valued responses of sea surface elevation and horizontal currents, respectively, and $i = \sqrt{-1}$.

Removing the explicit time dependence in the equations produces:

$$(\mu + i)u - \nu\,v = -\frac{g}{\sigma}\frac{\partial \zeta}{\partial x} \tag{5}$$

$$(\mu + i)v + \nu\,u = -\frac{g}{\sigma}\frac{\partial \zeta}{\partial y} \tag{6}$$

$$\zeta = \frac{ih}{\sigma}\left(\frac{\partial u}{\partial x} + \frac{\partial v}{\partial y}\right) \tag{7}$$

where

$$\mu = \frac{\gamma}{\sigma}; \quad \nu = \frac{f}{\sigma} \tag{8}$$

These equations, after some manipulation, can be arranged into second-order equations, producing:

$$\left(\frac{\partial^2}{\partial x^2} + \frac{\partial^2}{\partial y^2} + Q^2\right)(\zeta, u, v) = 0 \tag{9}$$

where

$$Q^2 = \frac{(1 - i\mu)^2 - \nu^2}{1 - i\mu}k^2 \tag{10}$$

with

$$k = \sigma/c \quad ; \quad c = \sqrt{gh} \tag{11}$$

In the above equation k is the wave number of the Kelvin wave in the absence of friction and c is the wave phase speed.

Form of solutions

Let x and y are the Cartesian coordinates chosen to be parallel to alongshore channel and cross-channel directions, respectively. Superscript d is used to denote in which sub-region variables are defined, for example, the water depth in sub-region d is denoted by h^d. The origin of the coordinates is defined at the northwestern corner as in Fang *et al.* (1991).

Following Taylor (1921), analytical forms of solutions in a channel to (9) are derived in two modes, one which satisfies.

$$v = 0 \quad \text{for} \quad 0 \le y \le B \tag{12}$$

another satisfying

$$v = 0 \quad \text{only at} \quad y = 0, B \tag{13}$$

In the above equations B is the width of the channel, and L is the length of the channel.

The constraint (12) gives Kelvin wave solutions as:

$$\zeta_{K-}^d = b_-^d \cdot \exp(\alpha^d y + i\beta^d x)$$

$$u_{K-}^d = \left(\frac{\beta^d h^d}{\sigma}\right)^{-1} b_-^d \cdot \exp(\alpha^d y + i\beta^d x)$$

$$u_{K-}^d = 0 \tag{14}$$

$$\zeta_{K+}^d = \left(\frac{\beta^d h^d}{\sigma}\right) b_+^d \cdot \exp(-\alpha^d y - i\beta^d x)$$

$$u_{K+}^d = b_+^d \cdot \exp(-\alpha^d y - i\beta^d x)$$

$$u_{K+}^d = 0 \tag{15}$$

while, the constraint (13) gives Poincare wave solutions:

$$\zeta_{P-}^d = \frac{ih^d}{\sigma} \sum_{n=1}^m \lambda_n^d (C_n^d \cos r_n y - D_n^d \sin r_n y) \cdot \exp(-s_n^d(l^d - x))$$

$$u_{P-}^d = \sum_{n=1}^m \lambda_n^d (-A_n^d \cos r_n y + B_n^d \sin r_n y) \cdot \exp(-s_n^d(l^d - x))$$

$$v_{P-}^d = \sum_{n=1}^m \lambda_n^d \sin r_n y \cdot \exp(-s_n^d(l^d - x)); \tag{16}$$

$$\zeta_{P+}^d = \frac{ih^d}{\sigma} \sum_{n=1}^m \chi_n^d (C_n^d \cos r_n y + D_n^d \sin r_n y) \cdot \exp(-s_n^d(x - l^{d-1}))$$

$$u_{P+}^d = \sum_{n=1}^m \chi_n^d (A_n^d \cos r_n y + B_n^d \sin r_n y) \cdot \exp(-s_n^d(x - l^{d-1}))$$

$$v_{P+}^d = \sum_{n=1}^m \chi_n^d \sin r_n y \cdot \exp(-s_n^d(x - l^{d-1})) \tag{17}$$

where l^d denotes the location of the interface between sub-regions d-1 and d and

$$\alpha^d = \frac{\nu k^d}{(1 - i\mu^d)^{1/2}}, \quad \beta^d = \frac{k^d}{(1 - i\mu^d)^{1/2}},$$

$$r_n = \frac{n\pi}{B}, \quad s_n^d = [r_n - (Q^d)^2]^{1/2}; \tag{18}$$

$$A_n^d = \frac{[(\mu^d + i)^2 + \nu^2] r_n s_n^d}{(\mu^d + i)^2 r_n^2 + \nu^2 (s_n^d)^2}, \quad B_n^d = \frac{\nu(\mu^d + i)^2 (Q^d)^2}{(\mu^d + i)^2 r_n^2 + \nu^2 (s_n^d)^2}$$

$$C_n^d = r_n - s_n^d A_n^d, \quad D_n^d = -s_n^d B_n^d \tag{19}$$

In the above equations the unknowns are b_-^d, b_+^d, χ_n^d and λ_n^d ($n = 1,2,...m$) where m is the numer of Poincare waves. The signs +/- denote the propagation directions to positive/negative x directions in the case of Kelvin waves, and similarly the directions of exponential decay in the case of Poincare waves.

Horizontal boundary conditions and matching interface conditions

Along the northern head we apply the condition

$$u^l = -r_0 \frac{c^l}{h^l} \zeta^l \tag{20}$$

which is a modified form of POBC.

In the study of Fang *et al.* (1991), the value of r_o was taken as zero at the portion of the impermeable barrier, representing the Shantung Peninsula and Ongjin peninsula, and a real-value between zero and one at the open portion. In more general cases it is noted that complex values are possible and a value larger than one might be chosen.

At the offshore open boundary the elevation information is given by

$$\zeta^{III} = \zeta_o \tag{21}$$

As an alternative to (21), we may define the normal velocity across the open boundary, or the combination of the elevation and velocity.

The continuity of sea surface elevation and flux are imposed at the interfaces between sub-regions. In detail, at the interface l^d, we have:

$$\zeta^{d-1} = \zeta^d$$

$$h^{d-1} u^{d-1} = h^d u^d \tag{22}$$

3. Results and Discussions

We represent the YS and the ECS covering the area between the Shantung and Ongjin Peninsulas to Ryukyu Islands as a finite channel of constant width with partial opening at the northern head, and full opening at the southern offshore region (Fig. 1). The Shantung Peninsula and Ongjin Peninsula at the northern head are represented as impermeable barriers. The lateral boundary of the channel is assumed to be fully closed.

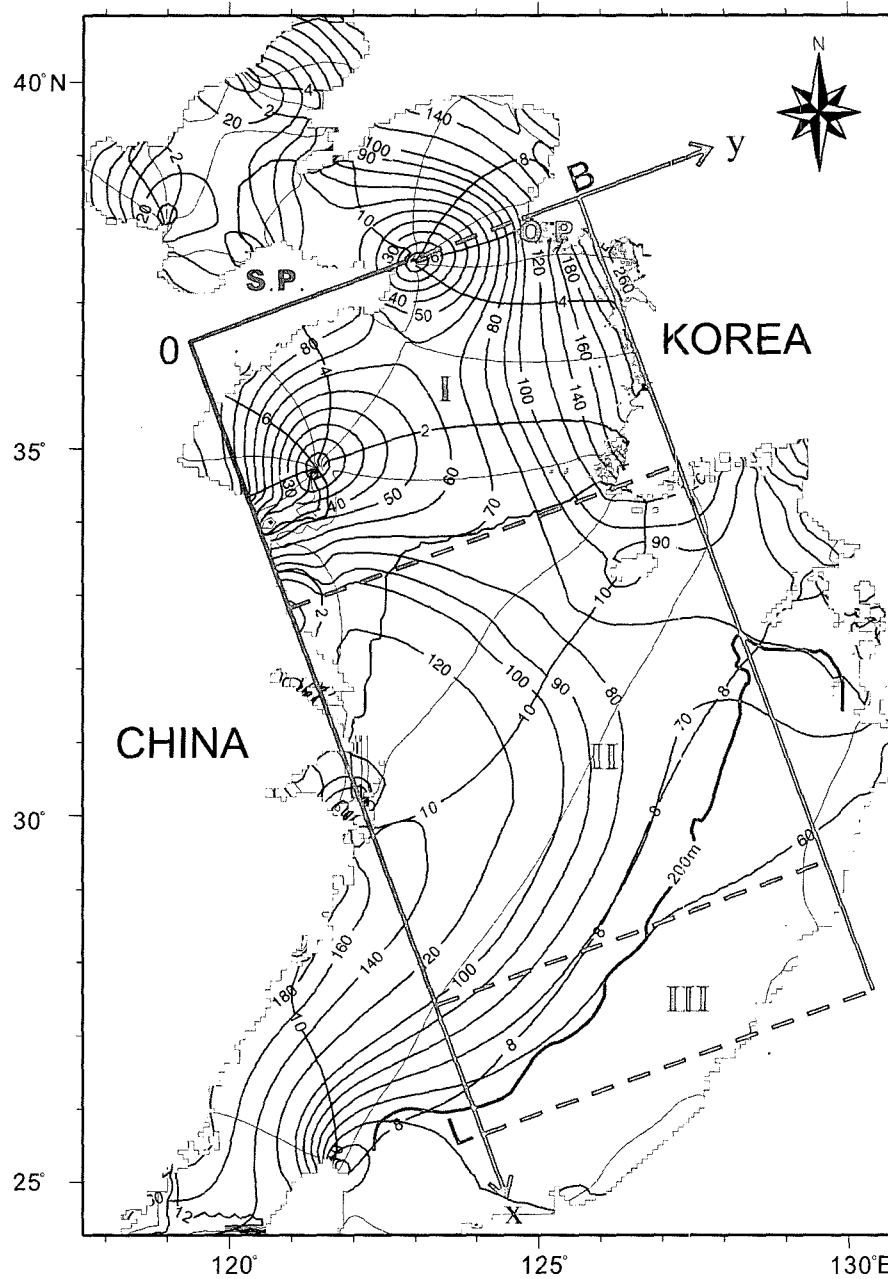A total of 3 sets of experiments have been performed in

Fig. 1. Schematized finite channel model region with three sub-regions for the analytic calculation of M_2 tide in the Yellow Sea and the East China Sea superimposed on the M_2 co-tidal chart computed numerically (KORDI 2002). S.P. denotes Shantung Peninsula, O.P. denotes Ongjin Peninsula. The blue line represents the 200 m depth contour.

this study. Throughout the calculations the width of the channel B is chosen as 600 km, the length of the channel L is chosen as 1450 km. The length of the three sub-regions are: $l' = 500$ km, $l'' = 750$ km, and $l''' = 200$ km, respectively. The depths in the three sub-regions are as base values taken as $h' = 45$ m, $h'' = 95$ m and $h'''=1000$ m which corresponds roughly to the average water depths of

the YS, ECS and Okinawa Trough, respectively, but the value of h'' varies in Exp. 1. The bottom frictional coefficient is fixed as 1×10^{-5} m/s in Exp. 1 and Exp. 3, while varying to 3×10^{-5} m/s and 5×10^{-6} m/s in Exp. 2 by taking into account the values used by Kang et al. (1999). Fang et al. (1991) used 1.5×10^{-3} m/s. The value of r_o is set to one, except for Exp. 3. Throughout the experiments f is fixed

to the value at the latitude of 30°N. Detailed values for the parameters used in each experiment are explicitly in figure captions.

At the offshore open boundary, the sea surface elevation is given as:

$$\zeta_o = 0.6\exp(-i \; 210/180\pi) \tag{23}$$

so that, along the offshore open boundary the M_2 tidal wave is assumed to have equal values of phase and amplitude.

With boundary conditions (20), (22) and (23), we could get simultaneous equations with $6(m+1)$ unknowns. The resulting matrix with complex-valued elements have been solved using a Collocation method as in previous analytical studies in the Yellow Sea. A total of 16 $(=m+1)$ Collocation points are defined along each of open boundaries and interfaces with equal intervals. A total of 9 Collocation points are allocated for Shantung Peninsula, while 2 Collocation points are identified for Ongjin Peninsula.

Exp. 1: Effects of water depth and contributions of each mode

We first examine the effects of changing the depths. For that, values of h^{II} are varied at 130 m, 95 m and 45 m, while values of h^{I} and h^{III} are fixed at 45 m and 1000 m, respectively. In the case of $h^{II}=45$ m, we note that the model is reduced to a two sub-region model.

From Fig. 2 it is apparent that patterns with two amphidromes characterize the tidal response in the western part of the model domain, which are formed primarily by the presence of an impermeable barrier representing the Shantung Peninsula. In the eastern part of the model domain, co-amplitude lines are more or less parallel to the lateral boundary of the channel with a maximum on the northeastern part, while the co-phase lines are roughly normal to the lateral boundary. Near the southern end of the sub-region II, we note that, due to the presence of abrupt changes in depth, splitted patterns appear in the distribution of co-amplitude lines. The variations in co-amplitude lines and co-phase lines are expected to be
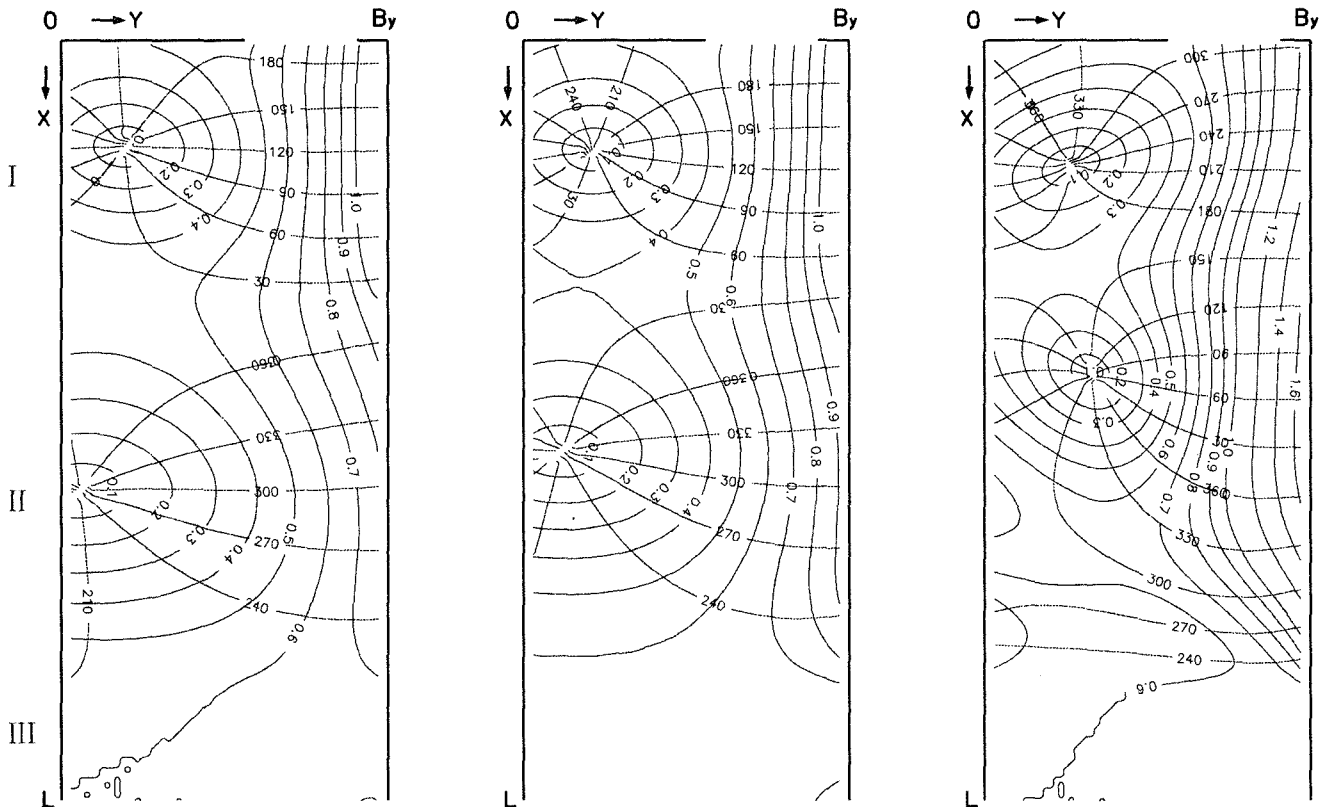

Fig. 2. Co-tidal charts computed with $\gamma=1\times10^{-6}$ m/s, $r_0=1.0$, $h^{I}=45$ m, and $h^{III}=1000$ m with a range of values of h^{II} (left: 130 m; middle: 95 m; right: 45 m). Co-amplitude lines are represented in units of 0.1 m when smaller than 1 m, while in units of 0.2 m when larger than 1 m. Co-phase lines are represented in units of 30°.
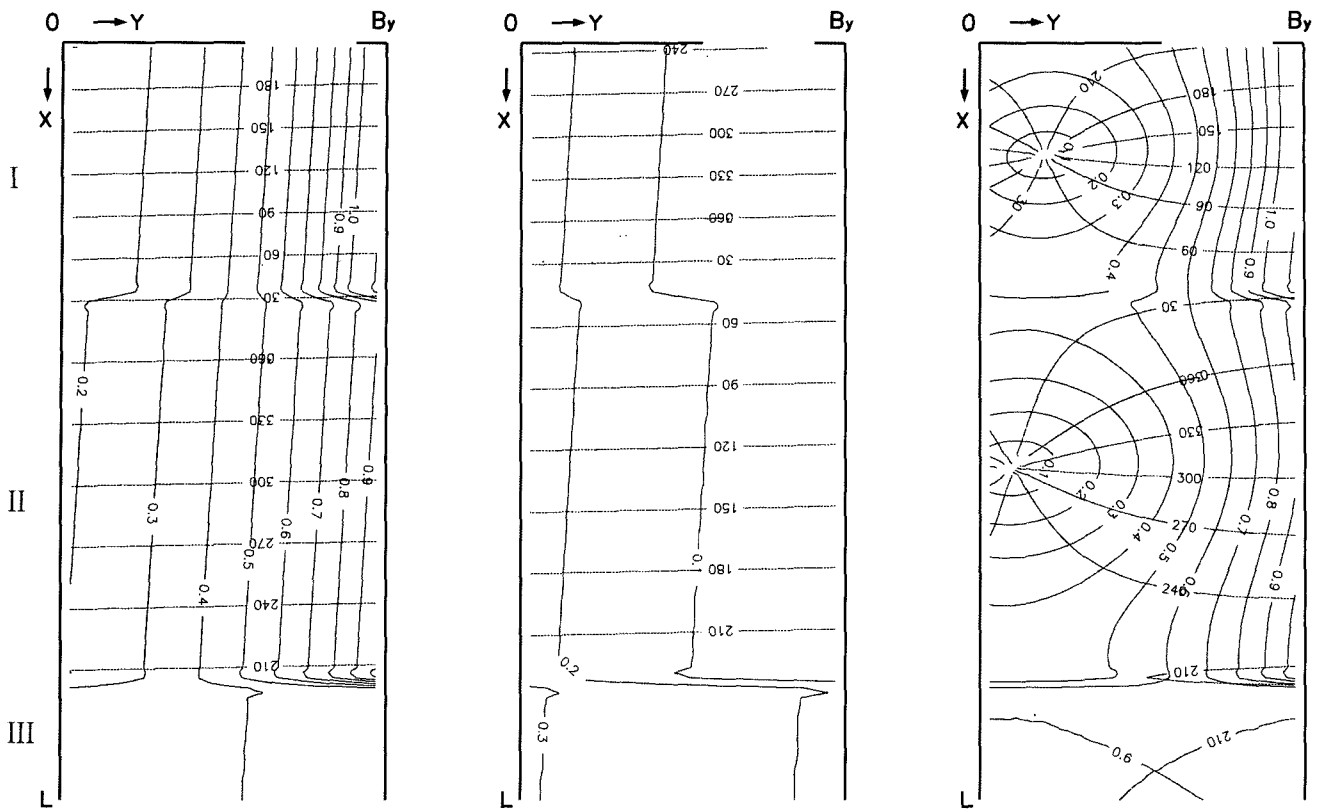
Fig. 3. Co-tidal charts of Kelvin waves computed with $\gamma=1\times10^{-6}$ m/s, $r_0=1.0$, $h'=45$ m, $h'=95$ m and $h'''=1000$ m (left: ζ_{K-}; middle: ζ_{K+}; right: $\zeta_{K-}+\zeta_{K+}$). Co-amplitude lines are represented in units of 0.1 m, while co-phase lines are represented in units of 30°.

very small in sub-region III, where the wave propagation speed is very large.

Increasing the value of h'' tends to shift the southern amphidrome to the west. Kang *et al.* (1999) noted that the bottom friction effectively shifts the amphidrome to the west, particularly the southern amphidrome. We may say that not only the bottom friction, but depth plays an important role in determining the location of the amphidrome. The northern amphidrome is affected to a relatively small degree according to the changes in h''.

It is also noted that the distance between the two amphidromes, which correspond to half of wavelength of the M_2 tidal wave, changes according to the value of h''. With an increase of h'' the northern amphidrome moves closer to the Shantung Peninsula and the western coastline, while the southern amphidrome moves further southward and closer to the western coastline. A change in the distance between the two amphidromes is expected because the tidal wave propagation is dependent upon the depth, that is, $c=\sqrt{gh}$.

Approaching the two sub-region models, the shape of the amphidromes becomes distorted and the overall tidal response increases but a maximum in tidal amplitude of more than 1.6 m occurs at the eastern coastline of sub-region II. In calculations with $h''=130$ m and 95 m, the maximum tidal amplitude occurs at the eastern corner of sub-region I, where it is more than 1.0 m.

Now, we will examine the relative contribution of Kelvin waves and Poincare waves. We have calculated the contribution of each mode for the case of $h''=95$ m.

Fig. 3 displays the co-tidal charts of the northward Kelvin wave, the southward Kelvin wave and their combined contribution. It is evident that the main feature of M_2 tide in the YS and the ECS can be reproduced by Kelvin waves. The northward Kelvin wave is responsible for the large tidal responses along the eastern coastline, while the contribution of the northward and southward Kelvin waves are more or less comparable near the western coastline. Two amphidromes are obviously formed as a result of the combined contribution of the two Kelvin waves but
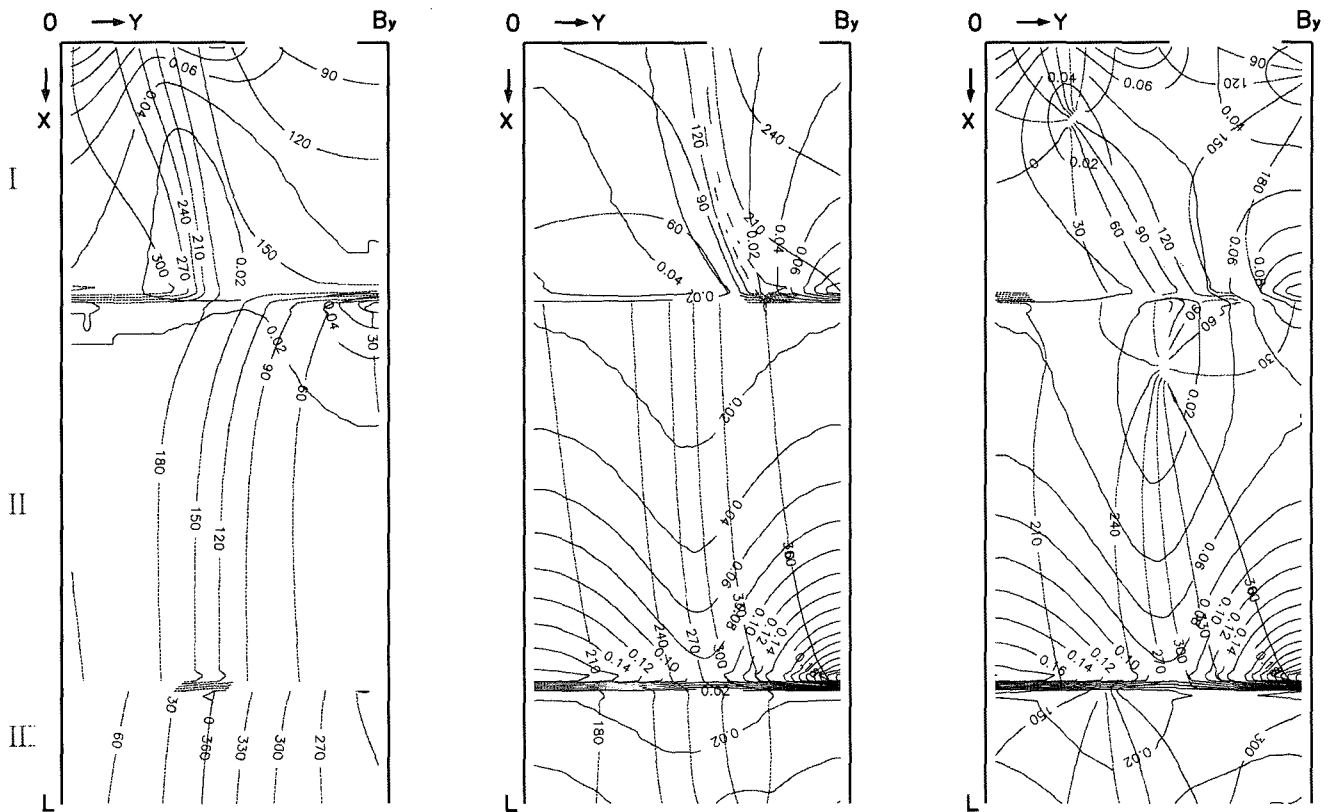
Fig. 4. Co-tidal charts of Poincare waves computed with $\gamma=1\times10^{-6}$ m/s, $r_0=1.0$, $h'=45$ m, $h''=95$ m and $h'''=1000$ m (left: ζ_{P-}; middle: ζ_{P+}; right: $\zeta_{P-}+\zeta_{P+}$). Co-amplitude lines are represented in units of 0.02 m, while co-phase lines are represented in units of 30°.

discontinuous changes in the co-amplitude lines appear due to the step-like variation in depths between the sub-regions. Physically the difference in wave numbers between sub-regions gives rise to the discontinuous changes at the interfaces.

Interesting features are noted in the change of co-amplitude lines as the Kelvin waves pass over the interfaces. In the eastern part of the model domain the amplitude of the northward Kelvin wave increases discontinuously, but in the western part decreases discontinuously. Within each sub-region, the amplitude decreases slowly as the wave goes northward. On the contrary, the amplitude of the southward Kevin wave increases discontinuously for all parts of the interfaces. Within each sub-region, the amplitude increases slowly as the wave goes southward.

Fig. 4 displays the co-amplitude and co-phase lines of the two Poincare waves and their combined contribution. It is noted that contributions of Poincare waves are substantially smaller than those of Kelvin waves and the overall patterns are much more complicated. Again the

discontinuous changes in the co-amplitude lines appear due to the step-like variation in depth between the sub-regions. We can see that Poincare wave evanescent southward are mostly trapped at the northwestern corner of sub-region I, while Poincare waves evanescent northward are mostly trapped at the southeastern corner of sub-region II. The combined contribution gives rise to amphidromic patterns near the northwestern corner of sub-region I and the middle of the northern part of sub-region II, while a degenerated form apppears in the northern end of sub-region III.

Exp. 2: Effects of bottom friction

Fig. 5 shows the effects of changing the frictional coefficient in sub-region II on tidal charts. It is evident that increasing the value of γ in sub-region II tends to shift the southern amphidrome to the west, and at the same time reducing the tidal amplitude response. With $\gamma=3\times10^{-5}$ m/s, the tidal amplitude at the northeastern corner reduces to less than 1m, while, with $\gamma=5\times10^{-6}$ m/s,

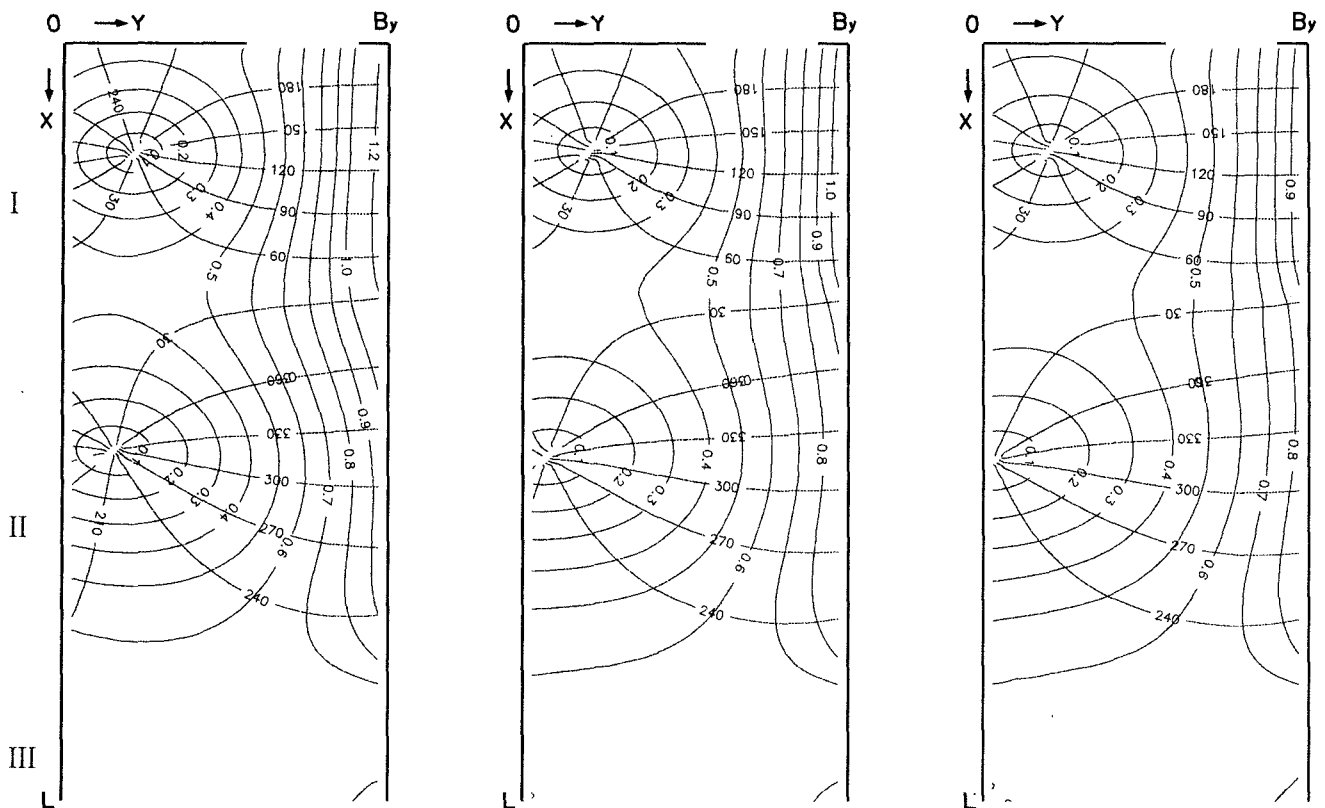**Fig. 5.** Co-tidal charts computed using r_0=1.0, h'=45 m, h''=95 m and h'''=1000 m with a range values of γ (left: 5×10^{-6} m/s; middle: 2×10^{-5} m/s; right: 3×10^{-5} m/s). Co-amplitude lines are represented in units of 0.1 m when smaller than 1 m, while in units of 0.2 m when larger than 1 m. Co-phase lines are represented in units of 30°.

larger than 1.2 m. The northern amphidrome is affected by a relatively small amount according to the change in γ. Fang *et al.* (1991) could reproduce tidal patterns in the YS with the use of a two-order larger value. It is surmised that the open boundary forcing might overwhelmingly determine the tidal response in a short channel model and thereby the damping could be less effective.

It is also noted that the distance between the two amphidromes changes. With an increase of the northern amphidrome moves closer to the Shantung Peninsula and the western coastline, while the southern amphidrome moves further southward and closer to the western coastline.

Exp. 3: Effects of the radiation factor r_0 at the northern open boundary

Keeping in mind that the outer domain north of the model domain is finite, Fang *et al.* (1991) claimed that use of a radiation factor between zero and one, modifying the POBC used by Kang (1984), might help to incorporate the reflected waves from the NYS. We however note that r_0

can be larger than one and even complex-valued. Three calculations have been carried out in the present study with values of r_0=0.5, 1.5 and 1.5exp ($i\pi$/6). A value of r_0=0.3 was taken in the calculation by Fang *et al.* (1991).

Comparing Fig. 6 (left) with Fig. 2 (middle), it is evident that use of a value smaller than one obviously gives rise to reflection at the northern open boundary between the Shantung peninsula and Ongjin Peninsula. However, there is no sign at all of an amphidrome forming near the tip of Shantung Peninsula. The co-amplitude lines become slanted but in the opposite manner shown in empirical tidal charts (for example, Nishida 1980) and numerical model results (for example, Choi 1980; Kang *et al.* 1991; Lee and Jung 1996). The southern amphidrome moves considerably to the west, manifesting a degenerated form, while the northern amphidrome moves closer to the northern coastline. Consequently, the distance between the two amphidromes increases significantly. Use of a value r_0=1.5 tends to produce patterns shown in empirical co-tidal charts and numerical model results. That is, the co-amplitude lines become slanted
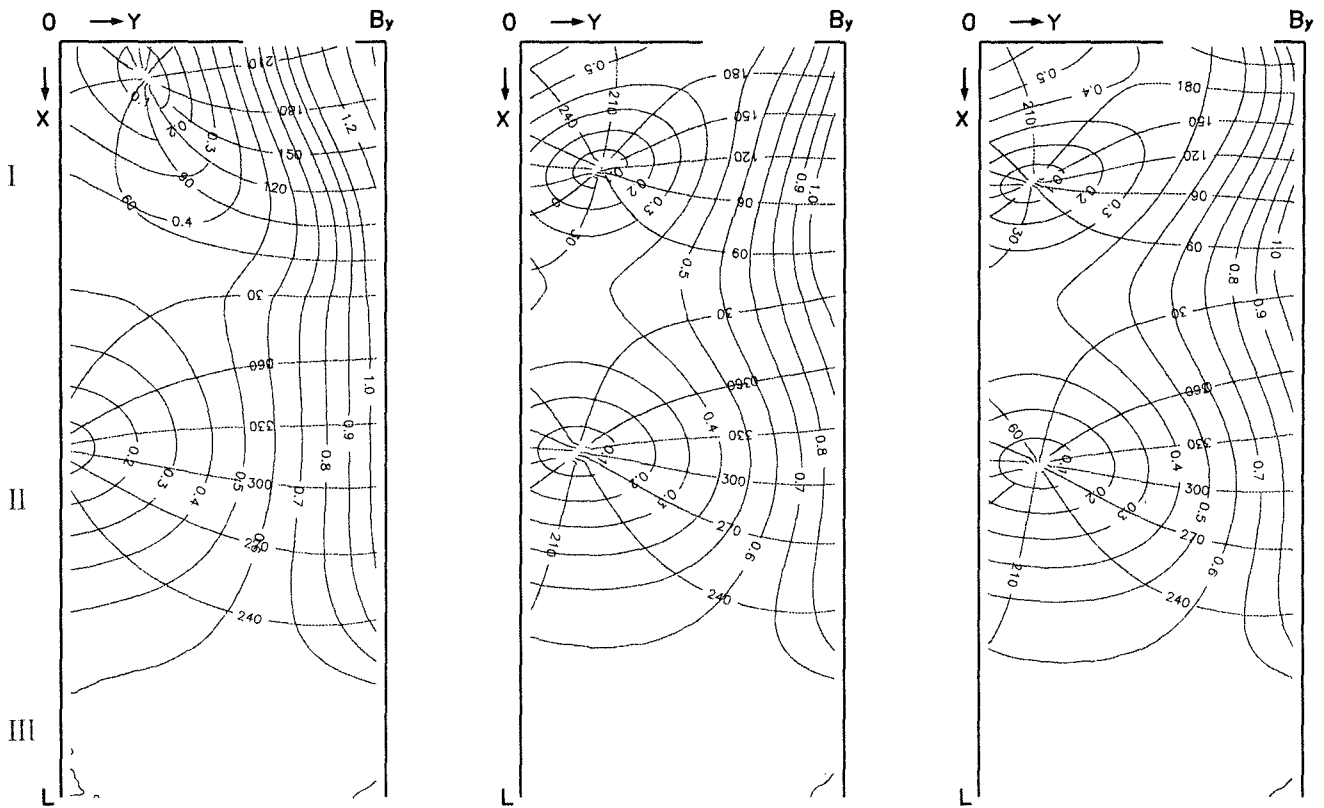
Fig. 6. Co-tidal charts computed using $\gamma=1\times10^{-6}$ m/s, $h'=45$ m, $h''=95$ m and $h'''=1000$ m with a range of values r_0 at the northern open head (left: $r_0=0.5$; middle: $r_0=1.5$; right: $r_0=1.5\exp(i\pi/6)$). Co-amplitude lines are represented in units of 0.1 m when smaller than 1 m, while in units of 0.2 m when larger than 1 m. Co-phase lines are represented in units of 30°.

to the east, which is opposite to the results obtained with $r_0=0.5$ (Fig. 6 middle). However, the tidal response at the northeastern corner decreases and the position of the maximal response moves southward. Compared with Fig. 2 (middle), the northern amphidrome is shifted to the south and the southern amphidrome to the east. Calculations of $r_0=1.5\exp$ ($i\pi/6$), which in addition takes into account phase shift, induces some further changes in co-tidal charts, especially near the northern open head (see Fig. 6 right).

5. Concluding Remarks

In this study we have presented an extended analytical model for the M_2 tide in the YS and the ECS which takes into account variations in channel depths in a step-like manner. The features of M_2 tidal distribution in the YS have been similarly produced as in previous models. In the ECS effects of depth changes are interestingly noticeable. In detail, due to the presence of an abrupt change in depth,

split patterns of M_2 tidal amplitudes occur in the ECS shelf region; co-amplitude lines tend to lie in the east-west direction near the end of sub-region II and the Poincare waves are pronounced on the shelf near the shelf edge.

A series of sensitivity experiments have shown that variations in depth, bottom friction and the open head boundary conditions all contribute to the determination of the formation of amphidromes as well as overall patterns of M_2 tidal distribution. We have seen that increasing water depths and bottom friction of h'' results in a westward shift of the southern amphidrome. Comparison of results with the empirical co-tidal chart or numerical result shown in Fig. 1) indicates that the present analytical model has failed to reproduce the tidal patterns in ECS in that there is a formation of amphidromic pattern with an amplitude change to the Chinese coast of an opposite nature. The amphidrome can be eliminated by modifying the depth, but the spatial tendency of the amplitude change cannot easily be reversed. It can be inferred that neglecting the lateral variation of water depth is responsible for the

discrepancy. The model results may be tuned to be more comparable with the known patterns in the ECS by prescribing a lateral variation in the amplitude and phase along the open boundary at the bottom of Ryukyu Islands. Sensitivity experiments, though not shown in this study, have shown that the tidal response is little changed unless a very large variation is considered. The tuning process is therefore not pursued in this study. Use of a radiation factor r_0 larger than one produces more realistic patterns near the northern open head than a use of r_0 factor smaller than one does. That is, use of a r_0 value smaller than one is not a proper way to incorporate the reflected waves from the NYS. A better way might be, though not considered in this study, to use the forced radiation conditions developed by Flather (1976). Instead of the elevation, the radiation conditions can be used at the southern open boundary. We have also suggested that the use of complex-valued radiation factor is possible. However, care must be taken in choosing a proper combination of the basic parameters (water depths, bottom friction and a radiation factors) in order to get more realistic tidal distributions than with previous models.

The proposed model is obviously an extension of previous models and gives more knowledge on M_2 co-oscillating tides in the YS and the ECS, but the channel width is assumed to be constant. Our immediate concern is therefore the development of a model with non-uniform width. Further studies will soon be completed, which take into account the variation in width in step-like manner.

Acknowledgements

References

Blumberg, A. and L. Kantha. 1985. Initial transients in long wave computations. J. Hydraul. Eng., 111(2), 237-255.

Brown, T. 1987. Kelvin wave reflection at the oscillating boundary with applications to the North Sea. Cont. Shelf Res., 7(4), 351-365.

Choi, B.H. 1980. A tidal model of the Yellow Sea and the eastern China Sea. Korea Ocean Research and Development Report 80-02, 72 p.

Flather, R.A. 1976. A tidal model of the northwest European continental Shelf. Memories de la Societe Royale des Science de Liege, 10, 141-164.

Fang, Z., A. Ye, and G. Fang. 1991. Solutions of tidal motions in a semi-enclosed rectangular gulf with open boundary condition specified. p. 153-168. In: Tidal hydrodynamics, ed. by B.B. Parker. John Wiley and Sons, Inc.

Godin, G. 1965. The M_2 tide in the Labrador Sea, Davis Strait and Baffin Bay. Deep-Sea Res., 12, 469-477.

Kang, Y.Q. 1984. Analytical model of tidal waves in Yellow Sea. J. Mar. Res., 42, 473-485.

Kang, S.K., J.Y. Chung, Y.Q. Kang, and S.-R. Lee. 1999. An analytical model of co-oscillating tide under frictional effect in the Yellow Sea. J. Oceanogr. Soc. Kor., 34, 22-35.

Kang, S.K., S.-R. Lee, and K.D. Yum. 1991. Tidal computation of the East China Sea and the East Sea. p. 25-48. In: Oceanography of Asian marginal seas, ed. by K. Takano. Elsevier.

KORDI. 2002. Study on tidal change prediction due to the large scale of coastal reclamation (TIDPRE) (II): Tidal prediction study for coastal flooding area of Korean Peninsula. Report prepared for National Oceanographic Research Institute (NORI). 291 p.

Lee, J.C. and K.T. Jung. 1996. Computation of M_2 tide for the Yellow Sea and the East China Sea using data assimilation. Ocean Res., 18, 13-24. (In Korean)

Nishida, H. 1980. Improved tidal charts for the western part of the North Pacific Ocean. Report of Hydrographic Researches, 15, 55-70.

Reid, R. O. and B.R. Bodine. 1968. Numerical model for storm surges in Galvaston Bay. ASCE J. Waterways and Harbor Div., 94, 33-57.

So, J.K. 2000. Analytical and numerical model studies of the M_2 tide in the Yellow Sea and the East China Sea. Ph.D. thesis, Seoul National University, Seoul. 131 p.

Taylor, G.I. 1921. Tidal oscillation in gulfs and rectangular basins. P. London Math. Soc., 2(30), 148-181.

Webb, D.J. 1976. A model of continental-shelf resonances. Deep-Sea Res., 23, 1-15.